Particle Nucleation for Dewetting Initiation of Thin Polymer Films

Ioannis Karapanagiotis,[1] William W. Gerberich[2]

[1]*"ORMYLIA" Art Diagnosis Centre, Ormylia, Chalkidiki, 63071, Greece*
[2]*Department of Chemical Engineering and Materials Science, University of Minnesota, Minneapolis, Minnesota 55455*

Received 11 August 2003; accepted 25 January 2005
DOI 10.1002/app.22028
Published online in Wiley InterScience (www.interscience.wiley.com).

ABSTRACT: A quantitative comparison between spontaneous dewetting and particle nucleation for thin (thickness = 17nm) polystyrene (PS) films on nonwettable silicon (Si) surfaces is presented both experimentally and theoretically. Performing experiments in a class 100 clean room, we found that ~ 23% of the observed dry patches formed because of dust particles, while the majority of the holes formed via the well known spontaneous dewetting process. The result was verified qualitatively by diffusion theory, which, however, predicted a diminished role for the airborne particles, leading to the conclusion that pre-existing particles on the Si surfaces and/or the polymer solutions contribute substantially to the dewetting process. The driving force of particle motion into the polymer film is examined by placing aluminum oxide (Al_2O_3) particles on PS films. Finally, the effect of particle geometry is studied by placing gold (Au) disks on the free surface of PS films. An optically continuous PS film is found to be present around the periphery of the disk particles, even after the completion of the dewetting process in the rest of the sample. An attempt to explain dewetting inhibition at the vicinity of the micro-disks, on the basis of molecular interactions developed in the system Au/PS/Si, is finally presented. © 2005 Wiley Periodicals, Inc. J Appl Polym Sci 98: 138–145, 2005

Key words: dewetting; coatings; atomic force microscopy (AFM); particle nucleation; polystyrene

INTRODUCTION

Thin polymer films (and coatings) find extensive use in industrial manufacturing. The processing of chips in the microelectronics industry includes polymeric photoresists with thickness range on the order of 1μm or even less.[1] Polymeric layers are used as lubricants on rigid disk magnetic media and polymers with low dielectric constant have been developed to be used in high performance micro-interconnects. Corrosion of metal components can be prevented by polymer coatings serving as physical and chemical barriers. Hydrophobic organic films are also used for the protection of cultural heritage objects from rainwater and atmospheric pollutants.[2–6] Finally, applications in paints, membranes, adhesives, and printing technology should be considered. All these applications typically require smooth and defect free polymer films.

Dewetting is a spontaneous self destructive process of the coating, leading to uncovering of the substrate. This prevents thin (thinner than a sessile drop flattened by gravity[7]) polymer films from serving the mentioned applications and, therefore, dewetting has attracted considerable attention.[8–11] Numerous contributions aiming to elucidate the dewetting process include studies on the stability of thin films,[12–19] investigations of the initiation mechanisms that lead to dewetting,[20–27] modeling and measurements of the lateral growth rate of the formed holes, usually called "dry patches," and studies associated with the evolution of the formed surrounding rim.[28–38] Other investigations, focused on the early dewetting stages, dealt with the assessment of a critical dry patch size (or critical film thickness) for lateral expansion and dewetting.[39–44]

As dewetting is most often a process to be prevented, several strategies that include substrate surface modifications, structural alterations of the polymer molecules, and utilization of additives, have been developed to minimize or even suppress dewetting, with very successful results.[45–55] On the other hand, controlled dewetting has been exploited as a surface-pattern process to fabricate ordered polymer and biomolecule arrays at the micrometer scale,[56–62] and to investigate properties of thin polymer coatings.[63–65]

Apart from the spontaneous dewetting, initiated by the unfavorable van der Waals interaction between the substrate and the film[13] or by inherent defects of the latter,[25] external parameters that affect the stability of the system, such as surrounding air composition,[66] or defects that affect the planar geometry of the film,

Correspondence to: I. Karapanagiotis (g.karapanagiotis@artdiagnosis.gr).

© 2005 Wiley Periodicals, Inc.

such as indents imposed by nanoindentation,[27,44] edge effects, and airborne particles,[23,27,34] can result in dewetting. Destabilizing substrate defects imposed prior to film deposition, like indents[27] and grains,[37] can have a similar effect, that is, nucleated dewetting. It has been recognized that upon heating above the glass transition temperature, Tg, of the polymer film, a surface particle can sink into the polymer and upon reaching the substrate, a dry patch starts to grow laterally.[23,27] Apparently, these particles differ from fullerene nanoparticles and additives that have been successfully applied as dewetting inhibitors in polystyrene/polybutadiene systems.[49,50,52]

Although the particle nucleation mechanism was identified relatively early, very little has been done to quantify its effect in the overall dewetting process.[23] Particles, however, can have truculent effects as they can initiate dewetting even in films thicker than 100nm (the cut off limit above which spontaneous dewetting does not occur) and deteriorate molecular patterns obtained by the dewetting process. In this study we perform a quantitative evaluation of the effect of airborne particles on the dewetting process of thin (thickness, $h = 17$nm) polystyrene (PS) thin films, spin cast onto silicon (Si) wafers, and compare our results with previously published data.[23] We also perform an effort to elucidate the origin of the particles found responsible for dewetting onset. We then discuss briefly the driving force for the particle motion inside the polymer film. Finally, we examine the effect of the particle shape, by placing gold (Au) disks on top of the PS films. The planar geometry (particle diameter $= 600\mu$m $\gg h = 17$nm) of the Au disks differs from that of a typical airborne particle. In this case one can consider that PS is placed between two hard surfaces (SiO_2 and Au).

EXPERIMENTAL

Monodisperse, low molecular weight PS (Mw = 10,900g/mol, Mw/Mn = 1.02, Polymer Labs, U.K.) was dissolved in spectroscopic grade toluene. Solutions of 1.0 wt % were spin coated onto 50mm diameter Si wafers, used as they were received from the supplier (Virginia Semiconductor, Fredericksburg, VA). Ellipsometric measurements of uncoated Si wafers revealed the presence of a 1.8nm thick native oxide layer. The orientation of the Si surfaces was $< 100 >$. Spin coating was performed in a class 100 clean room. Samples were then heated at 140°C, above the bulk glass transition temperature (Tg) of PS, to initiate dewetting. Heating was performed in a thermal chamber located inside the clean room, for 5 min. Samples were then cleaved into small pieces to fit in the 1 cm AFM holder. A Nanoscope III SPM (Digital Instruments, Santa Barbara, CA), operated in the contact mode, was used to image several formed dry patches and to reveal the presence (or not) of airborne particles on the surface of the exposed substrate. The airborne particle concentration was determined at several locations of the clean room, using an APC-1000 particle counter (Biotest Diagnostics Corp., Densville, NJ). The thickness ($h = 17$nm) of the PS films was determined by the AFM as the vertical depth of the formed dry patches and was verified by ellipsometry.

Aluminum oxide (Al_2O_3) particles with a nominal diameter of 0.05μm were deposited on the free surfaces of another set of PS coatings ($h = 17$nm) on Si. In this case, PS coatings were annealed at 60°C in vacuum to dry, that is, to remove residual solvent, prior to particle deposition. Oxide particles were deposited by simply placing the polymer films under a "cloud" of particle dust. The samples were then heated above Tg to initiate dewetting. A 5nm platinum (Pt) film was then deposited on the samples, and a Scanning Electron Microscope (SEM, Hitachi S-800) was used to image the formed dry patches.

Finally, gold (Au) disk particles were deposited on top of the PS coatings ($h = 17$nm) by thermal evaporation (Balzers, BAE 080 T) as follows: a dry, solvent free, PS coating on a Si wafer was placed inside the evaporator, and a mask was placed on top of the polymer surface. The mask was a Si wafer that carried circular openings (holes) with a diameter of $\sim 600\mu$m. This configuration resulted in the deposition of isolated Au disk particles, with thicknesses of 60nm and diameters $\sim 600\mu$m, on top of the PS surface. The deposition rate was 1.2nm/min. A highly pure Au (99.99%) target was used. The final obtained configuration was then Au($h_{Au} = 60$nm, $d_{Au} = 600\mu$m)/PS ($h = 17$nm, $d = 50$mm)/SiO_2 ($h_{SiO2} = 1.8$nm, $d_{SiO2} = 50$mm)/Si ($d_{Si} = 50$mm).

RESULTS AND DISCUSSION

Particle nucleation observation

Figure 1 presents typical AFM images that have been captured after heating a PS film above Tg. Along with the spontaneous indentlike surface disturbances that result in dry patches [Fig. 1(a)], particle induced patches are also formed [Fig. 1(b)]. Upon heating above Tg, airborne particles collect on the free surface of the film, sink into the polymer, and reach the substrate, and dewetting is initiated with the formation of laterally grown dry patches that expose the substrate to the air, as shown in Figure 1(b).[23,27] In contrast to Figure 1(b) where a bump-particle has been recorded at the center of the circular dry patch, in Figure 1(a) the revealed SiO_2 surface appears to be featureless. The observed (nano-)roughness of the revealed substrate surface can be attributed to polymer chains left behind the advancing rim. The obvious contrast of Figures 1(a) and 1(b) enabled us to distinguish dry patches formed as a result of a spontaneous nucleation mechanism from those formed because of particle presence.

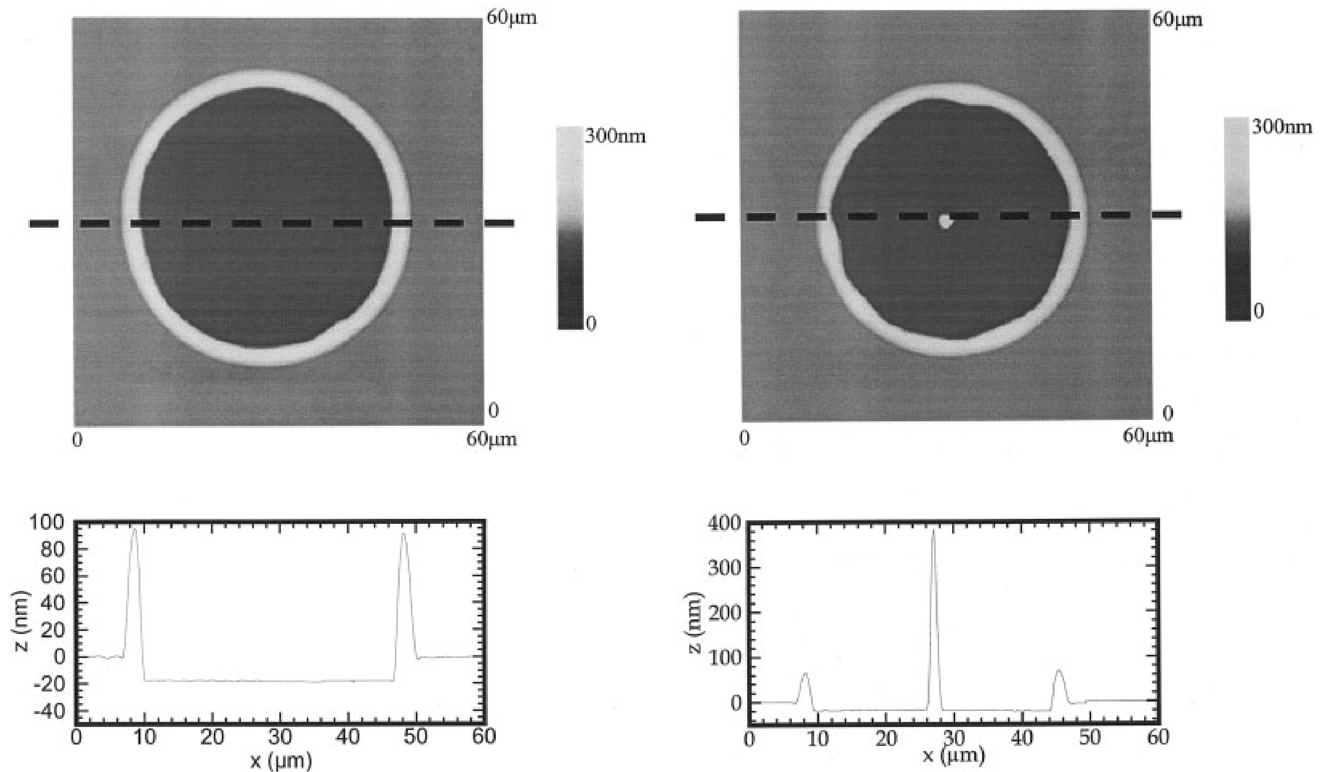

Figure 1 (a) AFM image and the corresponding cross section of a spontaneously formed dry patch. (b) AFM image and the corresponding cross section of a dry patch formed because of airborne particle. The particle is identified as a bump at the center of the revealed substrate.

Depending on its size, a particle sinks into the polymer either by gravity or by an attractive van der Waals interaction with the substrate, as is discussed later. Airborne particles may also deliver low surface energy contaminants on the free film surface, causing thus a surface tension gradient that can result in film rupturing.[9]

Quantification attempt of the dust particle nucleation process

In the following, a quantitative evaluation of the particle nucleation contribution to the overall detrimental dewetting process is attempted, and comparison with a similar study is performed.[23]

Table I provides airborne particle concentration measurements, for $\geq 0.3\mu m$ particles, that correspond to several locations inside the clean room (class 100) in which PS coatings were applied on three Si wafers and heated above Tg. As will be shown later, particles smaller than $0.3\mu m$ were found to be responsible for dewetting onset. The corresponding concentrations, n_0, for smaller particles ($0.1\mu m$ and $0.01\mu m$) were estimated as follows:[67]

TABLE I
Air particle concentration measurements, inside the clean room at several locations. Locations 1, 2, 3 and 4 are close to the spinner, used for sample preparation. Locations 5, 6 and 7 are close to the thermal chamber, used to heat the samples above T_g.

	Particle concentration, n_0 (part./ft^3)					
Location	$0.01\mu m$	$0.1\mu m$	$0.3\mu m$	$0.5\mu m$	$1.00\mu m$	$5.00\mu m$
1			125	105	35	0
2			165	105	40	0
3			745	335	115	0
4	eqs. 1 and 2		30	25	15	0
5			145	85	25	0
6			145	120	25	0
7			90	35	0	0
average	6444	1418	206	116	36	0

TABLE II
Comparison of dry patches formed spontaneously with ones formed by airborne particles, based on AFM images.

	Spontaneous dry patches	Particulate dry patches
sample 1	54	16
sample 2	57	13
sample 3	50	20

$$\frac{n_0(0.1)}{n_0(0.5)} = \frac{110}{9} \quad (1)$$

$$\frac{n_0(0.01)}{n_0(0.5)} = \frac{500}{9} \quad (2)$$

where $n_0(0.01)$, $n_0(0.1)$, and $n_0(0.5)$ are the particle concentrations for 0.01μm, 0.1μm, and 0.5μm particles, respectively. Equations (1) and (2) are valid for an at-rest clean room (class 10) and consequently can be applied in this study, performed in a fully operational clean room of class 100, only for estimating purposes.

Coatings were then cleaved to small pieces to fit in the 1cm AFM holder that was used to scan 70 dry patches. Spontaneous and particulate dry patches were recorded, and a quantitative comparison between the two is provided in Table II, for three wafers.[27] Holes formed because of particles represent ~ 23% of the total number of the investigated dry patches, which is higher (roughly by a factor of 4) than what was reported (particle nucleated holes ~ 6%) in a previous study,[23] where substantially lower airborne particle concentrations were reported. However, in both studies, spontaneous dewetting appears to be the dominant nucleation mechanism.

The number of aerosol particles (<1μm) that collect on a surface can be estimated by diffusion theory. The analysis is discussed in detail elsewhere.[68] The number of particles per unit area, N(t), that collect on a surface, can be calculated as:

$$N(t) = 2n_0 \sqrt{\frac{C_c k}{3\pi\eta} \frac{T}{d} \frac{t}{\pi}} \quad (3)$$

where t is the time that the surface is exposed to the aerosol with particle concentration n_0, k is Boltzmann's constant, T is the absolute temperature, η is the viscosity of the gas medium, d is the particle diameter, and C_c is the Cunningham slip correction factor to Stokes' Law, given by:

$$C_c = 1 + \left(\frac{\lambda}{d}\right)\left[2.514 + 0.8 \exp\left(-\frac{0.55d}{\lambda}\right)\right] \quad (4)$$

where d is the particle diameter and λ the mean free path of the gas molecules. For air at 1 atm and 20°C, λ_{20} = 66nm. For a given pressure $\lambda \sim T$ and therefore at 1 atm and 140°C, λ_{140} = 93nm. Using the average particle concentration, n_0, measurements shown in Table I, and eqs. (3) and (4), the number of particles collected by diffusion on a 50mm in diameter Si wafer can be calculated. The results are shown in Table III. The following values were used: T = 413.15 K, k = 1.38×10^{-23}J/K, $\eta = 2.38 \times 10^{-5}$ kg/m × s, the viscosity of air at 140°C,[69] and t = 5min, the time period that samples were exposed to the clean room air during heating above Tg. Spin coating was performed in only a few seconds, a period that can be considered as negligible. The results, shown in Table III, clearly underestimate the number of particles per wafer compared with the experimental results (Table II). Gravitational settling can be also calculated and taken into consideration, with a minor effect on the results of Table III. In any case, Table III does not predict the augmented role of the particle nucleation mechanism observed experimentally. Similar observation can be made in results achieved by Stange and coworkers.[23] The big difference observed in the data of Tables II and III can lead to the conclusion that dust particles present in the wafers prior to polymer deposition or in the applied polymer solution affect the results substantially. Consequently, any effort to suppress particle nucleated dewetting should focus primarily in an appropriate substrate surface and polymer solution preparation and cleaning. It should be noted, however, that eqs. (1) and (2), used to estimate the concentration of tiny particles, might be a source of error that affects the results of Table III.

Driving force for particle motion

Al_2O_3 particles (0.05μm), placed on top of polymer coatings, initiated dewetting at temperatures above Tg. Examining the samples with an optical microscope, an enormous increase in the density of the developed dry patches was observed compared with samples on which no particles were intentionally deposited. Using high resolution SEM images, the parti-

TABLE III
Calculation of the number of particles per wafer, collect by diffusion at 140°C, using equations 3 and 4. Wafer diameter was 50 mm.

Part. size	n_0 (part./m^3)	N (part./m^2)	part./wafer
0.01μm	227568	1257	2
0.1μm	50076	30	<1
0.3μm	7275	1.8	≪1
0.5μm	4097	0.7	≪1
1.0μm	1271	0.1	≪1
5.0μm	0	0	0

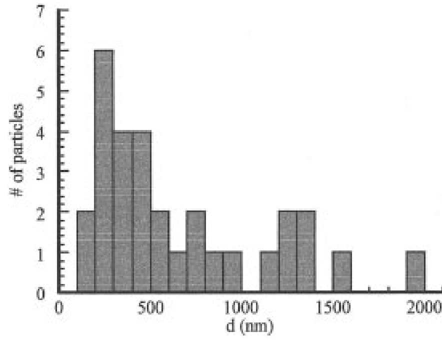

Figure 2 Size distribution of Al_2O_3 particles responsible for dewetting initiation.

cle size distribution was derived by measuring the dimensions of 30 particles, found at the centers of dry patches. The results are provided in Figure 2, which shows that clusters, rather than isolated Al_2O_3 particles, sunk into the polymer and initiated dewetting. It should be noted here that the measurements of Figure 2 may also contain dust particles, which, however, should represent only a tiny portion of the imaged particles.

Depending on the particle size, the dominant driving force for the vertical Al_2O_3 particle motion inside the film and toward the substrate can be either gravity or the van der Waals (VDW) attraction by the substrate wafer. Prior to particle sinking into the film, the former is given as follows:

$$F_{grav} = \frac{1}{6}\pi\rho g d^3 \tag{5}$$

where ρ is the density of the particle, g the gravitational constant, and d the particle diameter. The VDW force between a spherical particle and a surface, separated by a flat film, thickness h, is given by:[70]

$$F_{VDW} = \frac{H \bullet d}{12h^2} \quad (d \gg h) \tag{6}$$

where H is the Hamaker constant of the system particle/film/surface, which in our case is Al_2O_3/PS/Si. The presence of the native SiO_2 can be neglected because of its small thickness.[15] In this case, the Hamaker constant H is given by:[70]

$$H = \left(\sqrt{H_{Al_2O_3}} - \sqrt{H_{PS}}\right) \bullet \left(\sqrt{H_{Si}} - \sqrt{H_{PS}}\right) \tag{7}$$

where $H_{Al_2O_3}$, H_{PS}, and H_{Si} are the Hamaker constants of Al_2O_3, PS, and Si, respectively. Using: $\rho = 3.97 g/cm^3$ for Al_2O_3,[71] $H_{Al_2O_3} = 15.5 \times 10^{-20}J$, $H_{PS} = 6.3 \times 10^{-20}J$, $H_{Si} = 25.6 \times 10^{-20}J$,[72] and h = 17nm for the PS film thickness, we calculate that for particles with d $< 23\mu m$, $F_{VDW} > F_{grav}$ while for particles with d $> 23\mu m$, $F_{VDW} < F_{grav}$. The $23\mu m$ cut-off particle size is well above the documented sizes of Figure 2. Consequently, for the Al_2O_3 particles, VDW interaction, rather than gravity, is the force that drives the particle inside the polymer film. Both eqs. (5) and (6) are valid prior to particle motion towards the substrate, that is, when the film is flat and the separation distance between the particle and the substrate equals the film thickness, h. A higher VDW attractive interaction is expected upon particle sinking, compared with the one predicted by eq. (6), as the particle-substrate separation distance (i.e., the local film thickness) decreases.

Disk particles

Au disks were deposited on the surface of thin (h = 17nm) PS films. The deposition was performed by thermal evaporation. Using a mask with circular openings to cover the film surface, circular, isolated disk particles were developed on the free PS surface. Figure 3 shows the configuration obtained right after thermal evaporation [Fig. 3(a)] and the evolution of the system upon heating above the Tg of PS, at several annealing

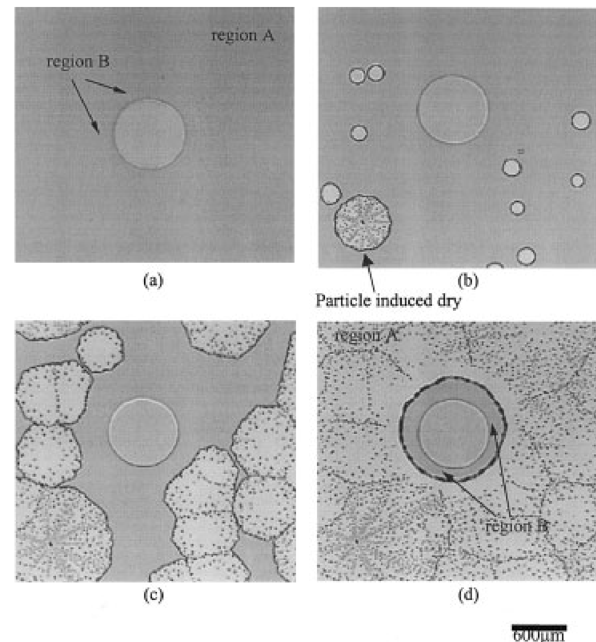

Figure 3 Evolution of a PS film (h = 17nm) on Si, upon heating at 140°C for several annealing times, t. A gold disk particle is present on top of the PS film, deposited by thermal evaporation. Micrographs correspond to: (a) t = 0, no thermal treatment above Tg; (b) t = 35 min; (c) t = 160 min; and (d) t = 1120 min. Region A corresponds to the film away from the particle and region B to the vicinity of the Au particle. In region A spontaneous dewetting and particle nucleation occurs. In region B a continuous PS film is present even after extensive heating (d).

times [Figs. 3(b-d)]. The thickness of the Au particle was 60nm. Upon heating, the standard dewetting process is observed away from the vicinity of the particle (region A) along with an optically visible particle induced patch. Dry patches are formed [Fig. 3(b)], exposing substrate to the air, and then they coalesce [Fig. 3(c)], resulting in droplets [Fig. 3(d)]. During this process, no evidence of dewetting is recorded at the vicinity of the Au particle (region B). On the contrary, a continuous PS film is present around the particle even after extensive heating [Fig. 3(d)]. Consequently, the presence of the Au particle results in dewetting inhibition in an area around its periphery. This optically unperturbed PS film is confined between the particle perimeter and a circular rim of accumulated polymer mass. AFM was used to scan region B before [Fig. 3(a)] and after [Fig. 3(d)] heating. Before thermal treatment the PS surface appeared to be smooth and featureless. Figure 4 shows an AFM image, taken in region B after extensive heating [Fig. 3(d)]. Here, the edge of the particle and a relatively large area of the surrounding PS film are shown. Several spontaneously formed indentlike disturbances can be distinguished at the surface of the PS film. In addition, a "wavelike" structure at the polymer free surface can be observed right next to the Au particle. Figure 5 shows schematically the structural evolutions. In the following, we provide possible explanations for the observations presented above.

The dewetting rate of PS from the Au surfaces is approximately 5 times higher than the corresponding rate of PS films placed on Si wafers.[36] A strong attractive VDW interaction between the Au particle and the

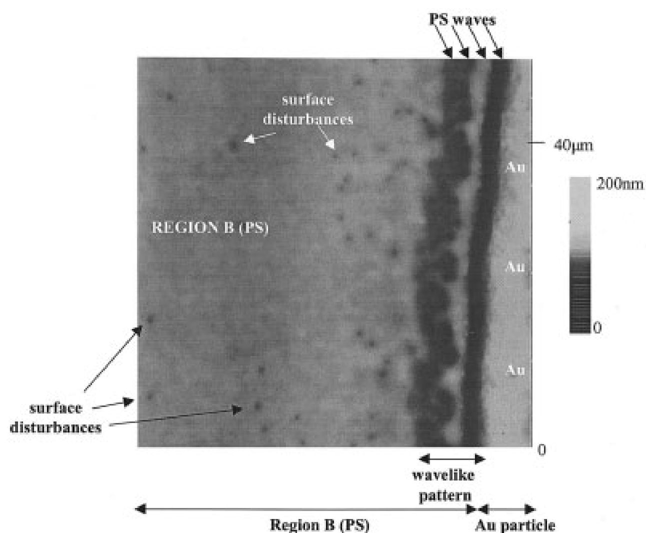

Figure 4 AFM image at the vicinity of the Au particle after extensive heating [region B, Fig. 3(d)]. The edge of the particle is shown. In the PS film numerous surface disturbances can be distinguished. Also, waves developed at the film surface next to the Au particle are observed.

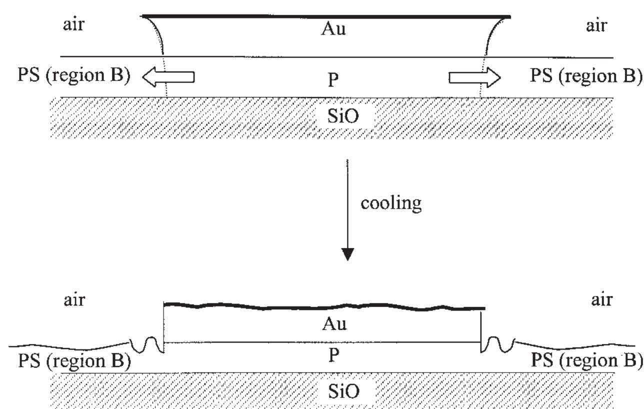

Figure 5 Schematic illustration of the structural changes in the system Au/PS. Upon cooling to ambient temperature, Au is placed under compressive stress, resulting in an increase of Au surface roughness. "Waves" at PS free surface next to the Au particle are observed. PS film thickness is exaggerated, compared to Au thickness.

Si substrate should also be expected. This interaction should force PS mass, initially present between the two hard surfaces, to squeeze out and to flow towards region B, upon heating above Tg. This flux opposes the growth of the indents that are spontaneously formed in region B, similar to region A, because of the unfavorable interactions with the Si substrate. The effect of this flux in region A can be considered negligible, as it is away from the Au particle. The rim of the accumulated polymer around region B is generated by the dewetting process, which occurs in region A. This rim cannot disintegrate to droplets because of the polymer mass coming from the region between the Au and the wafer. The attractive VDW interaction might be responsible for the wavelike structure developed at the periphery of the Au particle, as PS molecules forced to squeeze out of the region between the Au and the Si have to move to region B, which, however, is also a regime where unfavorable interactions (with the Si substrate) are developed. In addition, stresses developed because of the thermal expansion coefficient mismatch between Au and PS (and also SiO_2) and rising from the cyclic procedure heating at 140°C imaging at room temperature should also be considered. The difference in the thermal expansion coefficients between Au and PS (14.2×10^{-6}/°C and 79×10^{-6}/°C, respectively,[73]) places the Au film under compressive stress, upon cooling to ambient temperature. This results in a roughness increase of the free Au surface[74] by a factor of 3–5, as it was measured by AFM images of the free Au surface and might affect the formation of the wavelike structure shown in Figure 4 and presented schematically in Figure 5.

CONCLUSIONS

A quantitative comparison of spontaneous dewetting and particle nucleation was performed, exper-

imentally using AFM and theoretically using diffusion theory. Performing experiments in a controlled, class 100 clean room, environment characterized in Table I, we found that ~ 23% of the dry patches formed under the influence of airborne particles while the remaining 77% of the imaged dry patches appeared featureless. Spontaneous dewetting is the dominant rupturing mechanism for the conditions of the experiment. Diffusion theory underestimates the effect of airborne particles on the dewetting process, showing that pre-existing particles on the wafer surface and in the polymer solution contribute substantially to the dewetting scenario. A simple experiment was performed to measure the sizes of Al_2O_3 particles that acted as dewetting initiators. For the sizes found, it was shown that gravity is almost negligible compared to the VDW favorable interaction between the particles and the substrate. Therefore, VDW must be the driving force for particle motion towards the substrate, upon heating above Tg. Finally, it was shown that planar Au particles placed on top of PS films inhibit dewetting around their periphery. Consequently, particle shape (and size) highly affects the evolution process of thin polymer films upon annealing. Small particles act as dewetting initiators, while planar particles ($d_{particle} \gg h_{film}$) contribute to local dewetting inhibition.

Support by the Center for Interfacial Engineering (CIE), a National Science Foundation Engineering Research Center, is gratefully acknowledged.

References

1. Campbell, S. A. The Science and Engineering of Microelectronic Fabrication; Oxford University Press: New York, 1996.
2. Puterman, M.; Jansen, B.; Kober, H. J Appl Polym Sci 1996, 59, 1237.
3. Ciardelli, F.; Aglietto, M.; Montagnini di Mirabello, L.; Passaglia, E.; Giancristoforo, S.; Castelvetro, V.; Ruggeri, G. Prog Org Coat 1997, 32, 43.
4. Allesandrini, G.; Aglietto, M.; Castelvetro, V.; Ciardelli, F.; Peruzzi, R.; Toniolo, L. J Appl Polym Sci 2000, 76, 962.
5. Chiantore, O.; Lazzari, M. Polymer 2001, 42, 17.
6. Carretti, E.; Dei, L.; Baglioni, P. Langmuir 2003, 19, 7867.
7. Taylor, G. I.; Michael, D. H. J Fluid Mech 1973, 58, 625.
8. de Gennes, P. G. Rev Mod Phys 1985, 57, 827.
9. Kheshgi, H. S.; Scriven, L. E. Chem Eng Sci 1991, 46, 519.
10. Müller-Buschbaum, P. J Phys: Condens Matter 2003, 15, 1549.
11. Geoghegan, M.; Krausch, G. Prog Polym Sci 2003, 28, 261.
12. Sharma, A.; Ruckenstein, E. Langmuir 1986, 2, 480.
13. Brochard-Wyart, F.; Daillant, J. Can J Phys 1990, 68, 1084.
14. Sharma, A.; Reiter, G. J Colloid Interface Sci 1996, 178, 383.
15. Müller-Buschbaum, P.; Stamm, M. Physica B 1998, 248, 229.
16. Sharma, A.; Khanna, R. Phys Rev Lett 1998, 81, 3463.
17. Sharma, A.; Khanna, R. J Chem Phys 1999, 110, 4929.
18. Müller, M.; MacDowell, L. G.; Müller-Buschbaum, P.; Wunnike, O.; Stamm, M. J Chem Phys 2001, 115, 9960.
19. Reiter, G.; Khanna, R.; Sharma, A. J Phys: Condens Matter 2003, 15, 331.
20. Reiter, G. Phys Rev Lett 1992, 68, 75.
21. Reiter, G. Langmuir 1993, 9, 1344.
22. Müller-Buschbaum, P.; Vanhoorne, P.; Scheumann, V.; Stamm, M. Europhys Lett 1997, 40, 655.
23. Stange, T. G.; Hendrickson, W. A.; Evans, D. F. Langmuir 1997, 13, 4459.
24. Xie, R.; Karim, A.; Douglas, J. F.; Han, C. C; Weiss, R. A Phys Rev Lett 1998, 81, 1251.
25. Jacobs, K.; Mecke, K. R.; Herminghaus, S. Langmuir 1998, 14, 965.
26. Kim, H. I.; Mate, C. M.; Hannibal, K. A.; Perry, S. S. Phys Rev Lett 1999, 82, 3496.
27. Karapanagiotis, I.; Evans, D. F.; Gerberich, W. W. Langmuir 2001, 17, 3266.
28. Redon, C.; Brochard-Wyart, F.; Rondelez, F. Phys Rev Lett 1991, 66, 715.
29. Redon, C.; Brzoska, J. B.; Brochard-Wyart, F. Macromolecules 1994, 27, 468.
30. Brochard-Wyart, F.; de Gennes, P. G.; Hervert, H.; Redon, C. Langmuir 1994, 10, 1566.
31. Andrieu, C.; Sykes, C.; Brochard, F. J Adhes 1996, 58, 15.
32. Jacobs, K.; Seemann, R.; Schatz, G.; Herminghaus, S. Langmuir 1998, 14, 4961.
33. Ghatak, A., Khanna, R., Sharma, A. J Colloid Interface Sci 1999, 212, 483.
34. Hamley, L. W.; Hiscutt, E. L.; Yang, Y. W.; Booth, C. J Colloid Interface Sci 1999, 209, 255.
35. Reiter, G.; Sharma, A. Phys Rev Lett. 2001, 87, 166103.
36. Karapanagiotis, I.; Evans, D. F.; Gerberich, W. W. Colloids Surf A 2002, 207, 59.
37. Lorenz-Haas, C.; Müller-Buschbaum, P.; Kraus, J; Bucknall, D. G; Stamm, M. Appl Phys A 2002, 74, 383.
38. Masson, J. L.; Olufokunbi, O.; Green, P. F. Macromolecules 2002, 35, 6992.
39. Sharma, A.; Ruckenstein, E. J Colloid Interface Sci 1990, 137, 433.
40. Sharma, A. J Colloid Interface Sci 1993, 156, 96.
41. Sykes, C.; Andrieu, C.; Détappe, V.; Deniau, S. J Phys III France 1994, 4, 775.
42. Bausch, R.; Blossey, R.; Burschka, M. A. J Phys A: Math Gen 1994, 27, 1405.
43. Liu, H.; Bhattacharya, A.; Chakrabarti, A. J Chem Phys 1998, 109, 8607.
44. Karapanagiotis, I.; Gerberich, W. W.; Evans, D. F. Langmuir 2001, 17, 2375.
45. Henn, G.; Bucknall, D. G.; Stamm, M.; Vanhoorne, P.; Jérôme, R. Macromolecules 1996, 29, 4305.
46. Reiter, G.; Schultz, J.; Auroy, P.; Auvray, L. Europhys Lett 1996, 33, 29.
47. Feng, Y.; Karim, A.; Weiss, R. A.; Douglas, J. F.; Han, C. C. Macromolecules 1998, 31, 484.
48. Mounir, E. S.; Takahara, A.; Kajiyama, T. Polym J 1999, 31, 89.
49. Barnes, K. A.; Karim, A.; Douglas, J. F.; Nakatani, A. I; Gruell, H; Amis, E. J. Macromolecules 2000, 33, 4177.
50. Barnes, K. A.; Douglas, J. F.; Liu, D. W; Karim, A. Adv Colloid Interface Sci 2001, 94, 83.
51. Newby, B. Z.; Wakabayashi, K.; Composto, R. J. Polym 2001, 42, 9155.
52. Sharma, S.; Rafailovich, M. H.; Peiffer, D.; Sokolov, J. Nano Lett 2001, 1, 511.
53. Mackay, M. E.; Hong, Y.; Jeong, M.; Hong, S.; Russell, T. P.; Hawker, C. J.; Vestberg, R.; Douglas, J. F. Langmuir 2002, 18, 1877.
54. Yurelki, K.; Karim, A.; Amis, E. J.; Krishnamoorti, R. Macromolecules 2003, 36, 7256.
55. Li, X.; Han, Y.; An, L. Polymer 2003, 44, 5833.
56. Karthaus, O.; Gråsjö, L.; Maruyama, N.; Shimomura, M. Thin Solid Films 1998, 327–329, 829.

57. Zhang, G.; Yan, X.; Hou, X.; Lu, G.; Yang, B.; Wu, L.; Shen, J. Langmuir 2003, 19, 9850.
58. Zhang, Z.; Wang, Z.; Xing, R.; Han, Y. Surf Sci 2003, 539, 129.
59. Zhang, Z.; Wang, Z.; Xing, R.; Han, Y. Polymer 2003, 44, 3737.
60. Kim, Y. S.; Lee, H. H. Adv Mater 2003, 15, 332.
61. Luo, C.; Xing, R.; Han, Y. Surf Sci 2004, 552, 139.
62. Lee, L. T.; Leite, C. A. P.; Galembeck, F. Langmuir 2004, 20, 4430.
63. Reiter, G. Macromolecules 1994, 27, 3046.
64. Cole, D. H.; Shull, K. R.; Baldo, P.; Rehn, L. Macromolecules 1999, 32, 771.
65. Masson, J. L.; Green, P. F. Phys Rev E 2002, 65, 031806.
66. Bonnaccurso, E.; Butt, H. J.; Franz, V.; Graf, K.; Kappl, M.; Loi, S.; Niesenhaus, B.; Chemnitz, S.; Bőhm, M.; Petrova, B.; Jonas, U.; Spiess, H. W. Langmuir 2002, 18, 8056.
67. Sem, D. J. In Particle Control for Semiconductor Manufacturing; Donovan, R. P., Ed.; Marcel Dekker: New York, 1990; Chapter 6.
68. Leith, D. In Particle Control for Semiconductor Manufacturing; Donovan, R. P., Ed.; Marcel Dekker: New York, 1990; Chapter 2.
69. http://www.lmnoeng.com/Flow/GasViscosity.htm.
70. Evans, D. F.; Wennerström, A. The Colloidal Domain; VCH Publishers: New York, 1994.
71. Kittel, C. Introduction to Solid State Physics; Wiley: New York, 1996; 7th ed.
72. Visser, J. Adv Colloid Interface Sci 1972, 3, 331.
73. Barrett, C. R.; Nix, W. D.; Tetelma, A. S. The Principles of Engineering Materials; Prentice–Hall: Englewood Cliffs, NJ, 1973.
74. Huck, W. T. S.; Bowden, N.; Onck, P.; Pardoen, T.; Hutchinson, J. W.; Whitesides, G. M. Langmuir 2000, 16, 3497.